Journal of Power Sources 431 (2019) 250–258

Contents lists available at ScienceDirect

Journal of Power Sources

journal homepage: www.elsevier.com/locate/jpowsour

# Bio-inspired poly(3,4-ethylenedioxythiophene): Poly(styrene sulfonate)-sulfur@polyacrylonitrile electrospun nanofibers for lithium-sulfur batteries

Avinash Raulo [a], Sumana Bandyopadhyay [a], Salahuddin Ahamad [b], Amit Gupta [b], Rajiv Srivastava [a], Petr Formanek [c], Bhanu Nandan [a,*]

[a] Department of Textile Technology, Indian Institute of Technology Delhi, Hauz Khas, New Delhi, 110016, India
[b] Department of Mechanical Engineering, Indian Institute of Technology Delhi, Hauz Khas, New Delhi, 110016, India
[c] Leibniz-Institut für Polymerforschung Dresden e.V., Hohe Strasse 6, 01069, Dresden, Germany

## HIGHLIGHTS

- In-situ grown sulfur embedded in nanofibers are fabricated via electrospinning.
- Nanofibers supressed the shuttling phenomena by anchoring the polysulfides.
- Nanofiber incorporated cathode exhibit improved electrochemical performance.

## GRAPHICAL ABSTRACT

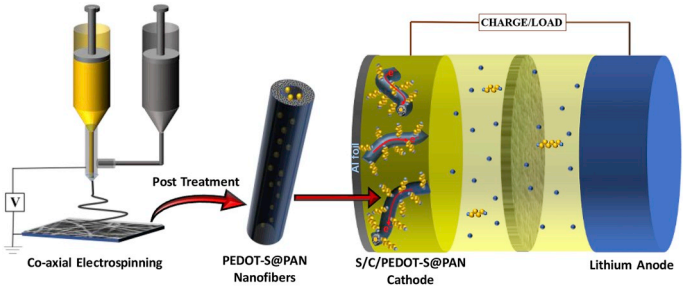


## ARTICLE INFO

*Keywords:*
Lithium-sulfur batteries
Electrospun nanofibers
Polysulfide
PEDOT:PSS
PAN

## ABSTRACT

The drive for commercializing high energy density lithium-sulfur batteries is leading to the development of various material architectures for suppressing the notorious "shuttle effect" of intermediate polysulfides and improve cycle life. Inspired by the structural features of plant roots protecting soil erosion, herein, we report a novel strategy to use poly(3,4-ethylenedioxythiophene):polystyrene sulfonate-sulfur@polyacrylonitrile electrospun nanofibers as flexible additives in the cathode of lithium-sulfur batteries to trap lithium polysulfides and suppress their dissolution into liquid electrolyte. The nanofibers consist of in-situ grown sulfur particles, embedded inside porous polyacrylonitrile shell and coated with poly(3,4-ethylenedioxythiophene):polystyrene sulfonate. The electrochemical performance of lithium-sulfur batteries using poly(3,4-ethylenedioxythiophene):polystyrene sulfonate-sulfur@polyacrylonitrile nanofiber incorporated sulfur hybrid cathode shows a significantly better cycle stability and excellent rate capability compared to the bare sulfur cathode owing to the adsorption effect of the nanofibers. Even after 500 cycles at a high rate of 0.5 C, the capacity retention is approximately 41% of the initial capacity with average columbic efficiency above 94%. This work offers a novel approach to fabricate viable lithium-sulfur batteries and possibly pave the way to further develop innovative flexible additives for practically applicable lithium-sulfur batteries.

* Corresponding author.
*E-mail address:* nandan@textile.iitd.ac.in (B. Nandan).

https://doi.org/10.1016/j.jpowsour.2019.05.055
Received 23 January 2019; Received in revised form 3 April 2019; Accepted 13 May 2019
Available online 22 May 2019
0378-7753/© 2019 Elsevier B.V. All rights reserved.

## 1. Introduction

The booming demand for high energy density battery systems spurred the development of lithium-sulfur batteries (LSBs), which offer theoretical energy density of 2600 Wh $kg^{-1}$ and an anticipated practical energy density of up to 500–600 Wh $kg^{-1}$, a value substantially higher than that of the state-of-art Li-ion batteries [1–3]. This high energy density is the result of two-electron reaction per sulfur as 16 Li + $S_8$ ↔ 8 $Li_2S$ at a standard potential of 2.2 V (vs $Li/Li^+$), providing a theoretical capacity of 1675 mAh $g^{-1}$ [2,4–7]. Although considerable amount of studies on this subject has been done, the commercialization of LSBs is still unsuccessful due to the severe capacity attenuation and short cycle life, which originates from the low electrical conductivity of sulfur and its discharge products $Li_2S_2/Li_2S$, and the dissolution and diffusion of intermediate lithium polysulfides ($Li_2S_{4\text{-}8}$) in liquid electrolyte during discharge-charge process known as the "shuttle effect" [8–10]. So far, several methods have been employed to address these problems. For instance, designing nanostructured cathodes by impregnating sulfur within conductive hosts such as porous carbon materials [11–16], polymers [17–19], metal oxides [20–24] have been extensively explored. Although such methods of physical encasement and chemical absorption of lithium polysulfides (LiPS) through the delicate designs endow the battery with excellent electrochemical performance, they cannot accomplish the goal for several reasons: First, the infusion of sulfur cannot ensure uniform distribution in the host and its content is also limited by such host structures, resulting in relatively low energy density. Second, the complicated fabrication techniques limit their large-scale industrial application. Since the essential requirement for battery design should be high mass loading of sulfur along with a facile fabrication method, in recent years much attention has been paid to the bare sulfur cathode [25]. Therefore, extensive research efforts have been put forward on inserting an interlayer between the bare sulfur cathode and separator [25–30], which alleviate the shuttle effect by absorbing the LiPS on the cathode side. Indeed, such approaches are highly promising and proven to be effective, however, the additional passive weight of the interlayer reduces the sulfur fraction in the whole system, which results in lowering the specific energy of the battery [5].

Considering these situations, the incorporation of functional additives in sulfur cathode at minimal concentration for cyclability enhancement might be regarded as an industrially amenable approach for improving the electrochemical performance of LSBs. In this respect, on-site adsorption by the metal oxide additives in sulfur cathode were found to be promising [31–36]. One of the early studies by Sung et al. reported that the addition of 15 wt% of nano-sized $Mg_{0.6}Ni_{0.4}O$ in sulfur cathode increased the initial specific capacity and cycle durability in comparison to the cells without additive, which was due to the improvement of LiPS adsorption on the additives [31]. Later on, various materials such as nano-sized $Al_2O_3$ [32], nano-sized $Mg_{0.8}Cu_{0.2}O$ [33], mesoporous $SiO_2$ [34], $BaTiO_3$ nanoparticles [35], $LiCoO_2$ [36] etc. were continually introduced as functional additives for sulfur cathode to restrain the LiPS dissolution. Although the incorporation of such additives could be considered as a simple and straightforward method to improve both the specific capacity and cycle life of LSBs, the rigid structure of metal oxides used in the aforementioned systems might not restrain the volume expansion problem of LSBs. Therefore, there is an urgent need for the development of flexible additives for sulfur cathode, which not only anchor the LiPS but also buffer the volume expansion during cycling of LSBs.

In this contribution, inspired by the role of fibrous plant roots in stabilizing the soil against flow erosion [37], herein, we report a novel approach of incorporating flexible nanofibers in sulfur cathode to hold the LiPS in position, protecting their dissolution and improving the cycle life of LSBs. Recently, electrospinning has been widely employed in the fabrication of nanofibers or microfibers of different materials with various assemblies due to its cost-effectiveness and relatively high production rate [38]. Through twining of the electrospinning process, controllable fibrous morphologies with high surface area and high surface-to-volume ratio, providing numerous active sites to hold the LiPS could be obtained. With this consideration, we fabricate core@shell structured electrospun nanofibers of in-situ grown sulfur core embedded inside porous polyacrylonitrile (PAN) shell (S@PAN). The nanofibers are then coated with a thin layer of poly(3,4-ethylenedioxythiophene): poly(styrenesulfonate) (PEDOT:PSS) to obtain conductive channels with a unique co-axial structure (PEDOT-S@PAN). The effect on LSB performance by direct incorporation of such nanofibers at minimal concentration as additives in sulfur cathode containing carbon black as conductive filler and sodium alginate as binder is studied. The electrochemical tests are conducted with cathode containing 40 wt% sulfur, since the capacity fade is severe in low sulfur loaded cathode [39] and therefore, it is expected to be a better choice to evaluate the LiPS dissolution inhibiting effect. Furthermore, the incorporation level of the additives should be of minimum level to achieve an industrially viable cathode. Therefore, only 5 wt% of PEDOT-S@PAN nanofibers were incorporated in the hybrid cathode. The rationale behind the use of sodium alginate as binder in this study is its mechanical rigidity, ionic conductivity and most importantly, it is an aqueous-based binder that avoid toxic N-methyl-2-pyrrolidone (NMP) as slurry solvent [40]. It is verified that the conductive PEDOT-S@PAN nanofibers provide a three-dimensional conductive network in the sulfur cathode that minimize the internal charge transfer resistance of electrode [41], meanwhile the PEDOT:PSS, PAN and encapsulated sulfur of the electrospun nanofibers act as LiPS anchors. Furthermore, the inclusive flexible fibrous structure buffer the volume expansion of sulfur cathode during cycling. More importantly, unlike the previously reported metal oxide-based additives, the plant root-like electrospun nanofiber additives are not inert to the redox reactions in LSBs due to the presence of encapsulated sulfur particles in the core. As a result, LSB with the incorporation of PEDOT-S@PAN nanofibers in sulfur cathode shows a significant improvement in cycle performance and rate capability as discussed herein.

## 2. Experimental section

### 2.1. Materials

Poly(acrylonitrile) (PAN) with Mw ~ 150,000 g $mol^{-1}$ (powder); Polystyrene (PS) with Mw ~ 192,000 g $mol^{-1}$ (beads); Poly(3, 4-ethylenedioxythiophene)-poly(styrenesulfonate) (PEDOT:PSS, 1.3 wt% dispersion in $H_2O$) were procured from Sigma-Aldrich. N, N-Dimethylformamide (DMF) (ACS reagent, ≥99.8%) and Oxalic acid were obtained from Fisher Scientific. Sodium thiosulfate pentahydrate ($Na_2S_2O_3.5H_2O$) was obtained from Merck. DI water used in the experiment was doubly distilled before use. Carbon black (TIMCAL Graphite & Carbon Super P-SUP) with BET nitrogen surface area of 62 $m^2g^{-1}$ was procured from Xiamen TOB New Energy Co. Ltd., China.

### 2.2. Fabrication of S@PAN nanofiber

The electrospinning was carried out by a co-axial vertical electrospinning setup (Physics Equipment Co. India) consisting of two syringe pumps, a high voltage power supply, a bilayer concentric spinneret and a flat piece of cardboard wrapped with aluminium foil as collector. All electrospinning processes were carried out under ambient conditions (25 ± 5 °C with a relative humidity of 49% ± 7%). In a typical procedure, 70 wt% $Na_2S_2O_3$ in DI water and 10 wt% PAN/PS (90/10) in DMF were used as core and shell fluid, respectively. The electrospinning process was carried out by fixing the spinneret-to-collector distance and applied voltage at 21 cm and 20 kV, respectively, together with a shell fluid flow rate of 1 ml/h and core fluid flow rate of 0.5 ml/h. After electrospinning, the nanofiber mats were carefully peeled off from the aluminum foil and post treatment was done by dipping the nanofibers in

chloroform for 4 h followed by dipping in aqueous solution of oxalic acid for an additional 4 h.

### 2.3. Preparation of PEDOT-S@PAN nanofibers

The as-obtained S@PAN nanofibers were coated with a thin layer of PEDOT:PSS by simple dip-and-dry method. The S@PAN nanofibers were first dipped into PEDOT:PSS solution and then added to ethanol/water solution (1:4, w/w) under continuous stirring. The solvents were then removed by placing nanofibers inside the vacuum oven at 60 °C.

### 2.4. Characterization

The subtle structure and morphology of the electrospun nanofibers were investigated by scanning electron microscope (SEM, Ultra 55, Carl Zeiss SMT, Jena, Germany) and high-resolution transmission electron microscope (HRTEM, JEOL 2100F). Energy-dispersive X-ray spectroscopy (EDS) was carried out to obtain the elemental mapping results. X-ray diffraction (XRD) patterns were investigated on a Rigaku Ultima IV diffractometer using Cu $K_\alpha$ radiation ($\lambda = 0.154$ nm). Fourier transform infrared (FTIR) spectra were recorded on a Nicolet iS50 spectrometer. The sulfur content was measured by thermogravimetric analysis with a TGA 4000 (PerkinElmer) analyzer under $N_2$ flow at a heating rate of 10 °C $min^{-1}$. The morphology of LSB cathode before cycling and after 100 galvanostatic discharging-charging cycle test at 0.1 C, recovered from the charged cells were investigated using FESEM (JSM-7800F, JEOL). The UV–Vis spectra were recorded by PerkinElmer Lambda 1050 spectrophotometer.

### 2.5. Electrochemical measurements

The cathode slurry was prepared by mixing 40 wt% elemental sulfur as active material, 5 wt% PEDOT-S@PAN nanofiber as additive, 45 wt% of conductive carbon black (Super P) and 10 wt% sodium alginate (Na-alginate) binder dissolved in DI water. The slurry was uniformly pasted on an aluminum foil, and then dried at 60 °C for 12 h under vacuum. The electrode films were cut into $\Phi = 12$ mm discs with approximately 2 mg $cm^{-2}$ mass loading of sulfur. For comparison, bare sulfur cathode was also prepared by mixing elemental sulfur, Super P carbon and Na-alginate binder in a weight ratio of 40:50:10 in DI water following a similar procedure and same sulfur areal mass loading as mentioned above. The electrolyte used consisted of 1 M bis(trifluoromethane)sulfonamide lithium salt (LiTFSI) dissolved in a mixture of 1,3-dioxolane (DOL) and 1,2-dimethoxymethane (DME) (1:1 by volume) with 1% $LiNO_3$ (TOB New Energy). A pure lithium foil was used as both counter and reference electrode, and Whatman glass fiber was used as separator. The two electrode cells were assembled in CR2016 coin-type test cells fabricated in an inert atmosphere glove box with the concentration of moisture and oxygen below 0.1 ppm. The cyclic voltammetry (CV) test at a scan rate of 0.1 mV $s^{-1}$ and the galvanostatic discharge-charge in the potential range of 1.7–2.8 V (vs $Li/Li^+$) at ambient temperature were performed using a Bio Logic BCS-810 electrochemical workstation. The current in the tests were varied from 0.1 C to 2 C (1 C = 1675 mA $g^{-1}$) and the obtained specific capacities mentioned in this article were calculated based on the mass of sulfur in the cathode. The electrochemical impedance spectroscopy (EIS) measurements in the frequency range of 100 kHz to 10 mHz with an AC voltage amplitude of 5.0 mV under the open-circuit condition were conducted on a Bio Logic VMP3 electrochemical workstation.

## 3. Results and discussion

The schematic illustration of the co-axial electrospinning process and fabrication of S@PAN nanofibers is shown in Fig. 1. The spinneret design is crucial for attaining robust and reproducible co-axial electrospun fiber [42]. The co-axial spinneret used in this work consist of two concentric metal capillaries promoting encapsulation of inner fluid by the outer fluid after ejection from the capillary nozzles. As explained in the experimental section, as a first step material, core@shell nanofibers were formed by taking PAN/PS in DMF solution as shell fluid and aqueous solution of $Na_2S_2O_3$ as core fluid. The key to successful co-axial electrospinning was ensuring that the inner-core fluid and outer shell-fluid form a compound Taylor cone and stay together in a concentric manner throughout the electrospinning process resulting in the formation of core@shell nanofiber with $Na_2S_2O_3$ core encapsulated in PAN/PS shell ($Na_2S_2O_3$@PAN/PS). Fig. 2a shows the low and high

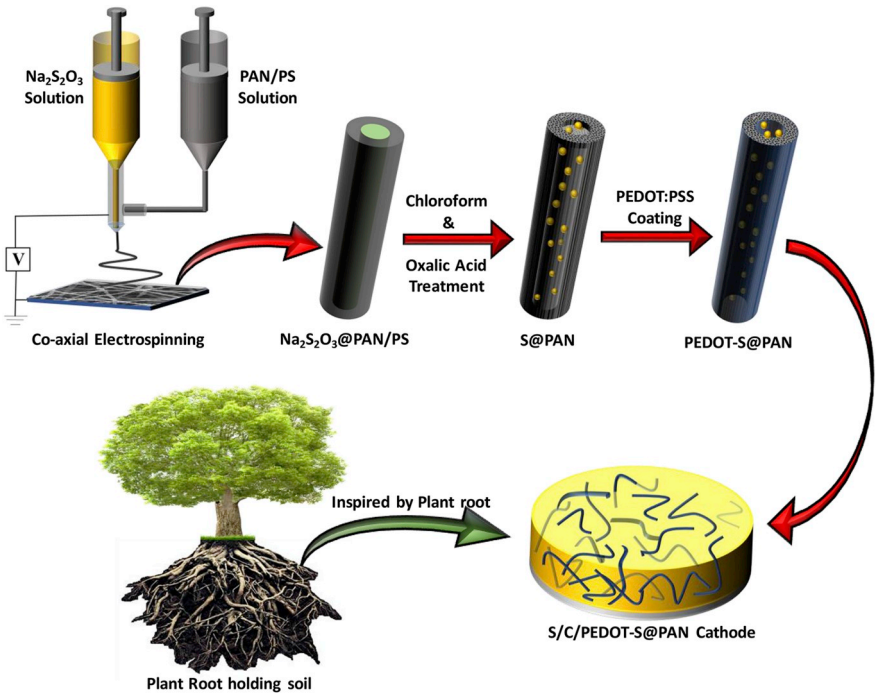


**Fig. 1.** Schematic illustration of plant root inspired design and fabrication of PEDOT-S@PAN electrospun nanofiber and its incorporation in LSB hybrid cathode.

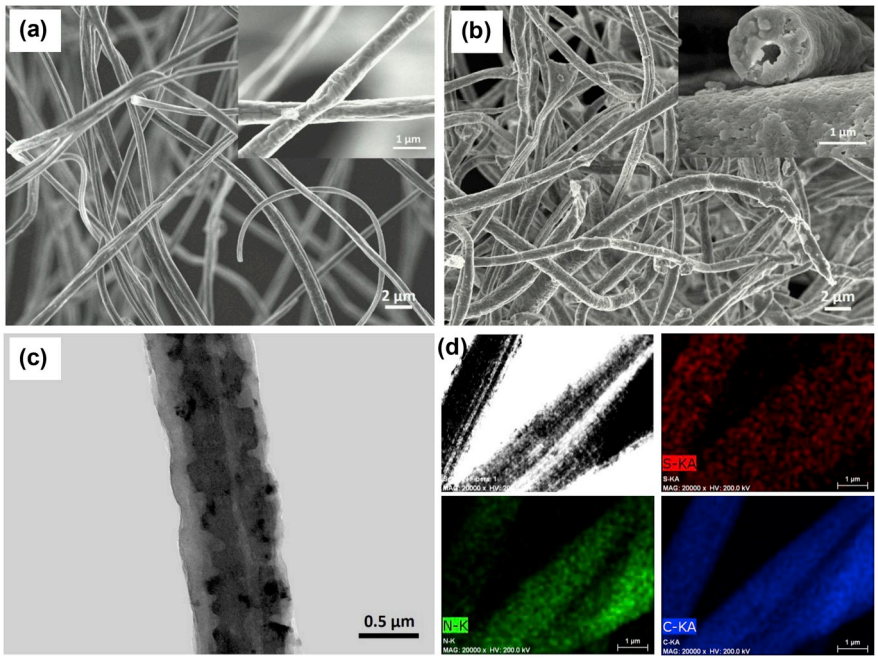


**Fig. 2.** SEM image of **a)** $Na_2S_2O_3$@PAN/PS nanofiber and **b)** S@PAN nanofiber; **c)** HRTEM image of S@PAN nanofiber, **d)** corresponding EDS mapping of sulfur, nitrogen and carbon.

magnification (inset of Fig. 2a) SEM images of the $Na_2S_2O_3$@PAN/PS nanofibers exhibiting uniform bead-free morphology. The post chloroform treatment of $Na_2S_2O_3$@PAN/PS nanofibers selectively etch the PS from PAN/PS shell and create porous PAN shell, which in-turn provide a path for the aqueous solution of oxalic acid to acidify $Na_2S_2O_3$ present in the core to precipitate sulfur. As observed by the SEM image shown in Fig. 2b, the morphological integrity of the nanofibers are preserved with apparent surface pores created by the post-treatment. The in-situ formation of sulfur in the core, generating sulfur encapsulated porous PAN (S@PAN) nanofiber involves the following reaction:

$$Na_2S_2O_3 + H_2C_2O_4 \rightarrow Na_2C_2O_4 + SO_2 \uparrow + H_2O + S\downarrow$$

The HRTEM image of S@PAN nanofiber shown in Fig. 2c revealed that the sulfur particles are distributed in the electrospun nanofiber. During the post-treatment, some of the sulfur particles appears to have percolated through the shell pores and settled along the cross-section of the nanofiber. This has been confirmed by the EDS elemental mapping of sulfur, nitrogen and carbon, as shown in Fig. 2d, where, the mapped elements could be observed uniformly along the nanofiber shape, confirming the uniform distribution of sulfur in the electrospun nanofibers. Moreover, the SEM images of S@PAN nanofiber longitudinal section (Fig. S1, Supplementary data) shows the distribution of sulfur along the longitudinal fiber axis.

The in-situ formation of sulfur in the electrospun nanofibers are further conferred by the XRD analysis as shown in Fig. 3. The diffraction peaks of sulfur particles synthesized by the oxalic acid treatment of aqueous solution of $Na_2S_2O_3$ could be indexed in accordance with the structure of elemental sulfur [43]. For $Na_2S_2O_3$@PAN/PS nanofibers, no characteristic peak of sulfur can be detected. However, diffraction peaks at two-theta angle of about 16.59° and 36.99° in case of S@PAN nanofibers are attributed to the sulfur crystal planes of (113) and (422), whereas absence of the other peaks confirm the encapsulation of sulfur in the electrospun nanofibers [44]. Furthermore, using TGA thermograms (Fig. S2, Supplementary data) the amount of sulfur present in the electrospun nanofibers are found to be ~11 wt% of the total fiber weight. This enabled the application of nanofibers as functional additives in sulfur cathode doesn't lead to a significant change in the total sulfur content in the cathode.

After PEDOT:PSS coating (PEDOT-S@PAN), the advantageous fibrous morphology is still preserved as illustrated by the SEM image shown in Fig. 4a. The HRTEM image in Fig. 4b shows that the thickness of PEDOT:PSS coating is approximately 25 nm. Moreover, the FTIR spectra (Fig. S3, Supplementary data) displayed distinctive transmittance evidence of PEDOT:PSS in PEDOT-S@PAN nanofibers by the presence of additional peaks compared to S@PAN at 1520, 1217, 924 and 680 $cm^{-1}$ that correspond to C=C, C–C, S–O, and C–S bonds, respectively, originating from the thiophene ring in PEDOT and the O-S-O signal at 1030 $cm^{-1}$ from the sulfonic acid group of the PSS chain [45, 46]. This further confirmed that the PEDOT:PSS was coated over the S@PAN surface in PEDOT-S@PAN nanofibers.

To manifest the hypothesis of "plant-root like traits of the electrospun nanofibers" as a proof-of-concept, the PEDOT-S@PAN nanofibers are directly added to bare sulfur and carbon black and mixed with Na-alginate in DI water solution to prepare hybrid cathode (S/C/PEDOT-

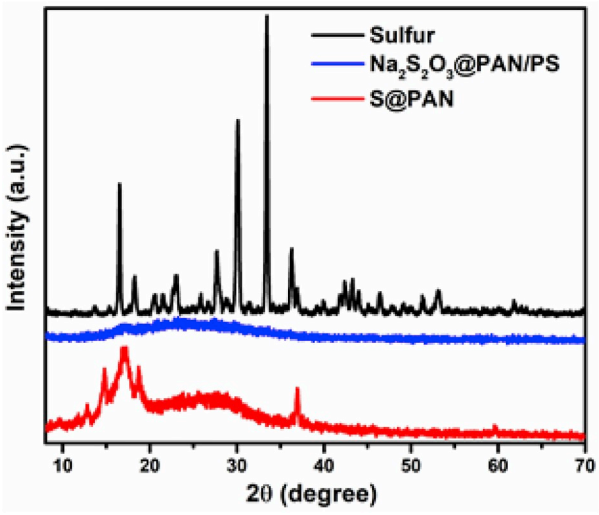


**Fig. 3.** XRD patterns of synthesized sulfur, $Na_2S_2O_3$@PAN/PS nanofiber and S@PAN nanofiber.

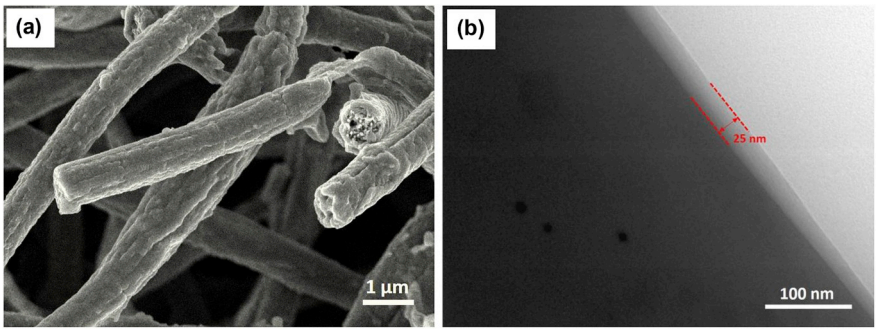


**Fig. 4.** **a)** SEM and **b)** HRTEM image of PEDOT-S@PAN nanofiber.

S@PAN) for LSB. Noticeably, the PEDOT-S@PAN nanofibers are uniformly distributed in the hybrid cathode with partial appearance on the surface of electrode (Fig. S4, Supplementary data) showing "plant root protruding out of the soil" like appearance. To probe the influence of PEDOT-S@PAN nanofiber incorporation on electrochemical properties of LSBs, a series of electrochemical measurements are carried out with S/C/PEDOT-S@PAN hybrid cathode. For comparison, bare sulfur-carbon black composite (S/C) cathode is also tested.

The initial CV profile of S/C and S/C/PEDOT-S@PAN electrodes shown in Fig. 5a indicates the impact of the PEDOT-S@PAN nanofibers on the redox reaction of the sulfur cathode. During the cathodic scan, both the electrodes display a pair of reduction peaks. The peak at ~2.3 V is attributed to the reduction of elemental cyclo-$S_8$ to the high-order LiPS ($Li_2S_n$, $4 \leq n \leq 8$) and the peak at ~2.0 V is due to the formation of insoluble low-order LiPS ($Li_2S/Li_2S_2$) [47]. However, the electrodes display significantly different oxidation behavior during the cathodic scan. The S/C/PEDOT-S@PAN hybrid cathode exhibit two overlapping oxidation peaks at ~2.35 V and ~2.40 V that can be assigned to the formation of the low-order LiPS and the high-order LiPS ($Li_2S_8$) or cyclo-$S_8$, respectively [14,27]. In contrast, S/C cathode exhibit only one oxidation peak at ~2.45 V corresponding to the formation of $Li_2S_2$ and $Li_2S_2$ to $Li_2S_8$ or cyclo- $S_8$. This difference might be attributed to the polarization caused by poor conductivity of S/C cathode [48]. In comparison to the S/C cathode, the S/C/PEDOT-S@PAN hybrid cathode shows a positive shift in reduction peak and negative shift in the oxidation peak, implying a decrease in cell polarization [49]. Meanwhile, the S/C/PEDOT-S@PAN hybrid cathode exhibit higher peak intensity and larger CV enclosed area than the S/C cathode, indicating the improvement in reactivity and LiPS redox kinetics by the incorporation of conducting PEDOT-S@PAN fibers [13]. Moreover, the CV curves of S/C cathode in the 1st to 7th cycle display a gradual decrease in peak intensities (Fig. 5b), whereas, the CV curve S/C/PEDOT-S@PAN hybrid cathode in the 1st and 7th cycle are well overlapped (Fig. 5c). This again confirms that the S/C/PEDOT-S@PAN hybrid cathode have an improved electrochemical reversibility [29].

The improvement in the electrochemical performance is further verified by galvanostatic discharge-charge test, performed at a constant current rate of 0.1 C. Fig. 6a shows the 1st and 100th galvanostatic discharge-charge profile of S/C and S/C/PEDOT-S@PAN electrodes, where the discharge curves exhibit two typical plateaus, consistent with the CV results shown above. Interestingly, S/C/PEDOT-S@PAN hybrid cathode shows lower polarization with the smaller voltage gap between the charge and discharge plateaus as compared to the S/C cathode. This might be due to the presence of surface conductivity of PEDOT-S@PAN nanofibers that improve the charge transport properties of hybrid cathode. The cycling performance of S/C and S/C/PEDOT-S@PAN electrodes measured at 0.1 C rate is presented in Fig. 6b. The initial discharge capacities of two electrodes were 683 and 739 mAh $g^{-1}$, respectively, which indicate the improvement in utilization of active materials by the addition of PEDOT-S@PAN nanofibers. Interestingly, the residual discharge capacity of S/C and S/C/PEDOT-S@PAN electrodes after 100 cycles are 265 and 433 mAh $g^{-1}$, with the corresponding capacity retention of 38.8% and 58.6%, respectively. This performance improvement in LSBs due to PEDOT-S@PAN nanofiber is further validated by incorporating different amounts (2.5 and 7.5 wt%) of nanofibers in LSB cathode and comparing with that of the S/C/PEDOT-S@PAN (i.e 5 wt% PEDOT-S@PAN in cathode) and S/C electrode. As shown in Fig. S5 (Supplementary data), even with the addition of 2.5 wt% PEDOT-S@PAN nanofibers (S/C/PEDOT-S@PAN-2.5), a small improvement in initial capacity with a significantly improved capacity retention after 80 cycles as compared to S/C cathode was observed. At 5 wt% nanofiber (S/C/PEDOT-S@PAN) the improvement in initial capacity and cycle stability is further catalyzed. However, 7.5 wt% PEDOT-S@PAN nanofiber incorporation (S/C/PEDOT-S@PAN-7.5) leads to marginal negative effect with a low initial capacity and cycle stability as compared to S/C/PEDOT-S@PAN hybrid cathode which might be due to the agglomeration of nanofibers at higher concentration. These values suggest that the incorporation of small amount of PEDOT-S@PAN nanofibers with bare sulfur not only increases the initial capacity but improves the cycling stability, which is also reflected

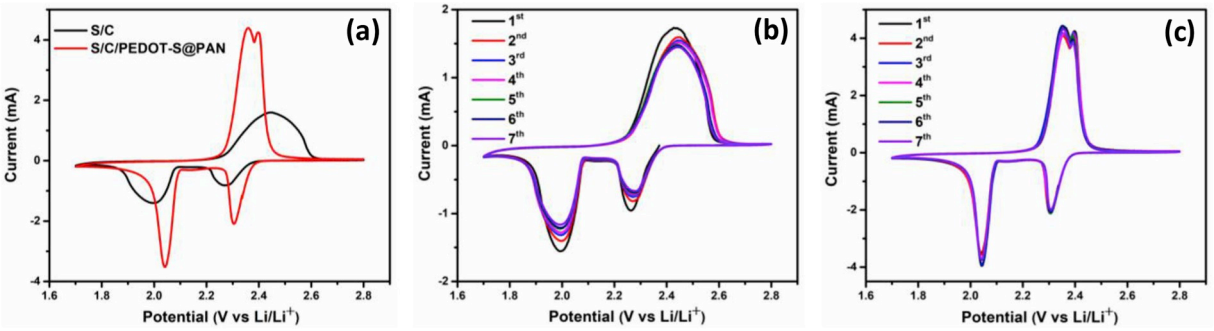


**Fig. 5.** Cyclic voltammograms of **a)** 1st cycle of S/C and S/C/PEDOT-S@PAN electrode, **b)** Initial 7 cycles of S/C cathode, **c)** Initial 7 cycles of S/C/PEDOT-S@PAN hybrid cathode.

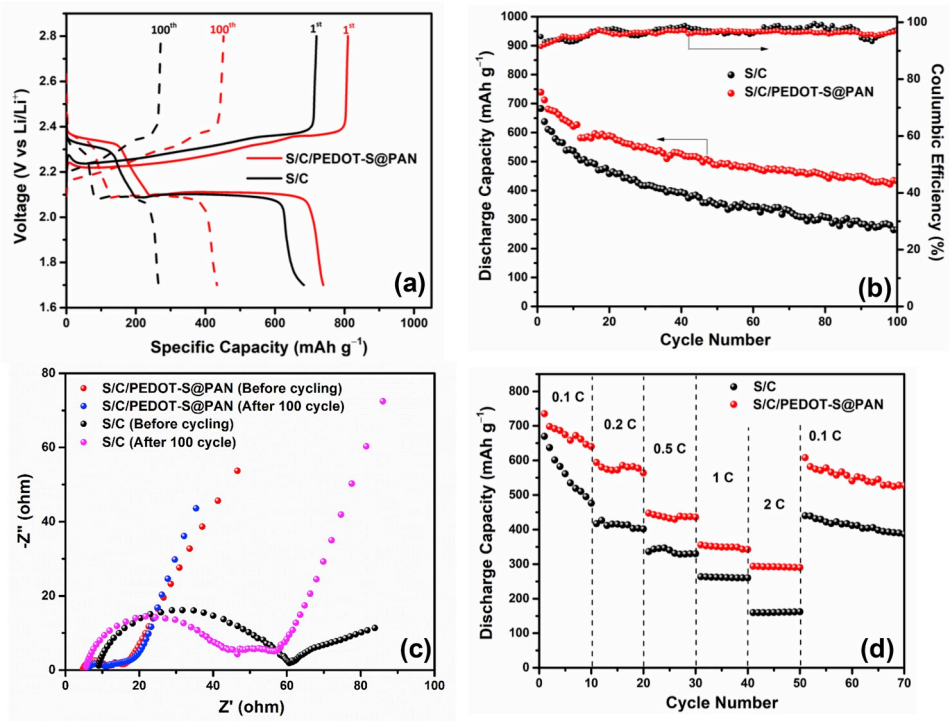


**Fig. 6.** **a)** Galvanostatic discharge-charge voltage profile and **b)** Cycling performance at 0.1 C rate; **c)** Nyquist plots before and after 100 cycles, **d)** Rate capabilities at various rates of S/C and S/C/PEDOT-S@PAN electrodes.

in the 1st and 100th discharge-charge profiles in Fig. 6a.

To better understand the electrochemical kinetics, which is closely related to charge-transfer in the electrode, EIS analysis of S/C and S/C/PEDOT-S@PAN electrodes are also carried out before and after 100 cycles. As shown in Fig. 6c, the Nyquist plot of S/C/PEDOT-S@PAN hybrid cathode before and after cycling displayed depressed semicircle at high-medium frequencies than that of the S/C cathode. The diameters of these semicircles representing the charge-transfer resistance ($R_{ct}$) at the electrode/electrolyte interface shows a lower value for S/C/PEDOT-S@PAN hybrid cathode due to the enhancement of conductivity. This suggest that the incorporation of PEDOT-S@PAN nanofibers in the hybrid cathode ensure a fast electron transfer, resulting in a faster reaction kinetics. This favorable effect is also reflected in the rate performance of the LSBs, tested with fresh set of coin cells with same compositions. As shown in Fig. 6d, the S/C cathode deliver discharge capacities of 670, 417, 336, 263, 159 mAh $g^{-1}$ at 0.1, 0.2, 0.5, 1 and 2 C, respectively. When the current return to 0.1 C, a discharge capacity of only 440 mAh $g^{-1}$ (~65.6% of initial discharge capacity) is regained. On the other hand, S/C/PEDOT-S@PAN hybrid cathode deliver discharge capacities of 735, 594, 447, 355 and 294 mAh $g^{-1}$ at 0.1, 0.2, 0.5, 1 and 2 C, respectively. Moreover, a reversible capacity of 607 mAh $g^{-1}$ is restored when the current decrease back to 0.1 C, approaching ~82.6% of its initial discharge capacity.

The effect on overpotential by the incorporation of PEDOT-S@PAN nanofibers is also evaluated by quantifying the magnitude of overpotential $\eta$ at constant current $i$ for S/C and S/C/PEDOT-S@PAN electrodes according to $\eta = (V - V_{OCP} - iR_{int})$, where $V_{OCP}$ is the open circuit potential and $R_{int}$ is the internal cell resistance [50]. The typical open circuit potential (OCP) curve corresponding to thermodynamic equilibrium state is obtained at 0.01 C-rate in the voltage range of 1.7–2.8 V vs. Li./$Li^+$. It is well known that the increase in current leads to the higher overpotentials and results in low specific capacity [51]. Therefore, both the electrodes (S/C and S/C/PEDOT-S@PAN) were cycled at 0.2 C-rate in the voltage range of 1.7–2.8 V vs. Li/$Li^+$ and the potential profiles were compared to that of the OCP curve as shown in Fig. S6 (Supplementary data). The potential profiles show a significant difference in overpotential during charging/discharging for both the electrodes. A small overpotential has been observed in the case of S/C/PEODT-S@PAN hybrid cathode while significantly higher overpotential witnessed in case of S/C cathode. The lower value of overpotential during charging/discharging profile of S/C/PEDOT-S@PAN hybrid cathode compared to the S/C cathode is ascribed to a higher delithiation/lithiation amount in the electrode resulting in a higher specific discharge capacity.

To further understand the improvement in electrochemical performance by the incorporation of PEDOT-S@PAN nanofibers, the morphological changes of S/C/PEDOT-S@PAN hybrid cathode before and after 100 cycles of galvanostatic discharging-charging at 0.1 C-rate are investigated using ex-situ FESEM. The PEDOT-S@PAN nanofiber protrusion in the hybrid electrode before cycling (Fig. 7a) shows the as-fabricated morphology without any interaction with the active material components of the electrode. In contrast, the PEDOT-S@PAN nanofiber protrusion after 100 cycles display the rough surface due to the material deposits over the nanofiber (Fig. 7b and Fig. S7, Supplementary data). The EDX elemental mapping of cycled hybrid cathode shows pronounced signal of carbon, sulfur and oxygen distributed along the PEDOT-S@PAN nanofiber (Fig. S8, Supplementary data). This reveals that the material deposits over the nanofiber surface might be the mixture of electrolyte and LiPS [52]. Apparently, the LiPS dissolved in the electrolyte and shuttled from sulfur cathode to Li anode after cycling can also be evaluated by characterizing the separator and Li anode. As shown in Fig. S9 (Supplementary data), after 50 cycles of discharging-charging at 0.1 C-rate, lower amount of LiPS residue is observed on the separator of S/C/PEDOT-S@PAN hybrid cathode than S/C cathode ascertained by the visual observation of the cycled separator as well as the UV–vis spectra of DOL/DME (1:1 vol) solution after dipping the cycled separators in it. This is also correlated with EDX spectra of the cycled Li-anode (Fig. S10, Supplementary data) showing lower amount of sulfur shuttled and accumulated on the surface of Li anode in case of S/C/PEDOT-S@PAN hybrid cathode compared to S/C cathode. This validate the ability of PEDOT-S@PAN nanofibers to anchor the LiPS and restrict its shuttling effect.

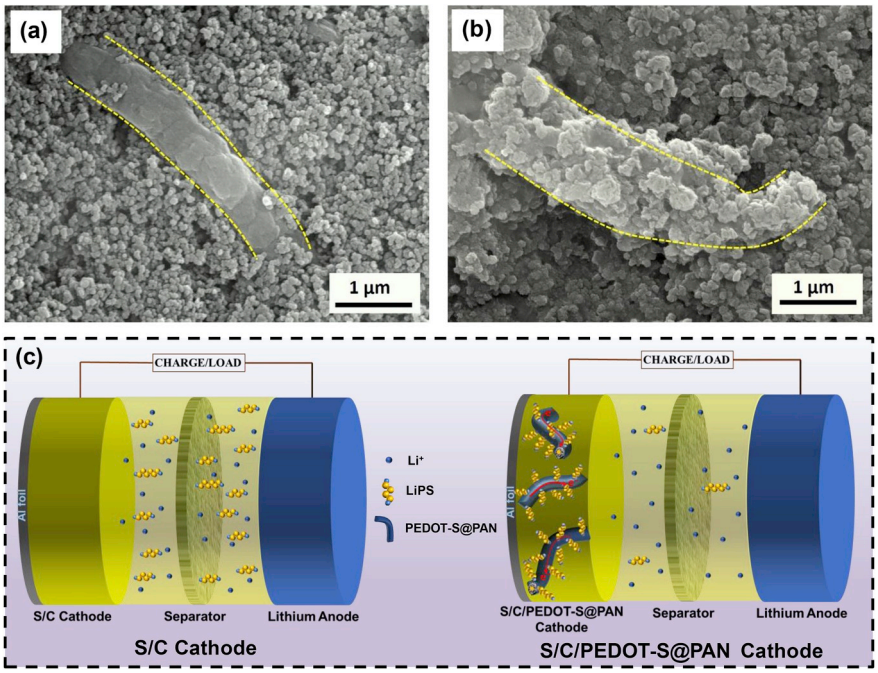


**Fig. 7.** FESEM image of S/C/PEDOT-S@PAN hybrid cathode **a)** before and **b)** after 100 cycles of galvanostatic discharging-charging at 0.1 C; **c)** Schematic illustration of LiPS dissolution inhibiting effect by the PEDOT-S@PAN nanofibers.

Furthermore, in order to obtain better insight into the importance of PEDOT-S@PAN nanofiber architecture in improving the electrochemical performance, galvanostatic discharge-charge experiment is carried out at 0.1 C-rate with a cathode containing 40 wt% sulfur with incorporation of same amount (5 wt%) of PEDOT:PSS coated mono-axial PAN nanofibers (S/C/PEDOT-PAN). As shown in Fig. S11 (Supplementary data), the S/C/PEDOT-PAN cathode deliver an initial discharge capacity of 730 mAh $g^{-1}$, a value slightly less than that for S/C/PEDOT-S@PAN hybrid cathode, but much higher than that for S/C cathode. After 100 cycles, the electrode retains a discharge capacity of 348 mAh $g^{-1}$ (47.6% of initial capacity). The improved discharge capacity and cycle life of S/C/PEDOT-PAN cathode compared with S/C cathode might be due to the following reasons: First, the presence of conductive PEDOT:PSS coating in PEDOT-PAN nanofibers imparted LiPS anchoring sites through the polar-polar interaction of its electron rich functional groups (thiophene) and LiPS [53]. Second, the nitrile group of PAN nanofiber containing lone pair of electrons might interacted with LiPS through a coordinate bond-like interaction [54]. Moreover, the significant improvement in cycle life of S/C/PEDOT-S@PAN hybrid cathode compared with S/C/PEDOT-PAN cathode reveal that the encapsulated sulfur could indeed bind with the external LiPS through the surface pores and restrict its dissolution during the continual cycling. In order to further assure the importance of in-situ synthesized sulfur in the nanofibers, three different cells each of S/C/PEDOT-PAN and S/C/PEDOT-S@PAN cathode are discharged-charged at 0.1 C-rate and their average discharge capacity with error bars indicating standard deviation are presented in Fig. S12 (Supplementary data). This infer that the sulfur encapsulated in the nanofibers could indeed improve the cycling performance. The comparisons of initial discharge capacity and the discharge capacity after cycling of different cathodes are summarized in Table 1. This indicates the individual intrinsic advantages of each component of PEDOT-S@PAN nanofiber (PEDOT:PSS, PAN and encapsulated sulfur) to afford a strong LiPS anchoring effect, suppressing its dissolution in the liquid electrolyte and thereby significantly improving the cycling stability of LSB. In contrast, LiPS formed in S/C cathode can easily dissolve in the electrolyte and cause severe shuttle effect, leading to a fast performance deterioration as illustrated schematically in Fig. 7c.

**Table 1**
Comparison of discharge capacity of S/C, S/C/PEDOT-PAN and S/C/PEDOT-S@PAN electrodes before and after cycling.

| Electrode | Initial discharge capacity (mAh $g^{-1}$) | Discharge capacity after 100 cycles at 0.1C (mAh $g^{-1}$) |
|---|---|---|
| S/C | 683 | 265 |
| S/C/PEDOT-PAN | 730 | 348 |
| S/C/PEDOT-S@PAN | 739 | 433 |

Based on the above results, long-term performance of S/C/PEDOT-S@PAN hybrid cathode is evaluated by discharging-charging at a higher current of 0.5 C. The hybrid cathode still could deliver an acceptable discharge capacity of 408 mAh $g^{-1}$ and maintained capacity retention of ~40.4% after 500 test cycles (Fig. 8). More importantly, columbic efficiency above 94% is maintained during the long cycle measurement.

With all the above demonstrations, the significant improvement in LSB performance by the incorporation of PEDOT-S@PAN nanofiber additives can be attributed to the following reasons: (i) the conductive PEDOT:PSS framework of PEDOT-S@PAN nanofibers could solve the

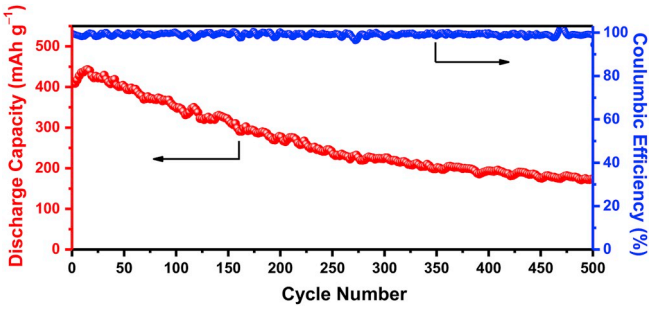


**Fig. 8.** Galvanostatic discharge-charge voltage profile of S/C/PEDOT-S@PAN hybrid cathode at 0.5 C.

problem of the low electrical conductivity of sulfur, (ii) at the same time, the PEDOT-S@PAN nanofibers acted like an expansion buffer zone due to its elastic fibrous nature, preventing the cathode from further fracture, and (iii) most importantly, each component of the nanofiber, such as PEDOT:PSS, PAN and encapsulated sulfur could anchor the external LiPS and restrict their dissolution during the continual cycling. Indeed, the direct comparison of our obtained capacity values with the previously reported values is difficult due to the difference in conditions of measurements, and the performance of batteries are amalgamation of various factors. Typically, the higher specific capacity values of sulfur cathode correlate with the high specific surface area of the conductive carbon used [55]. However, most of the sulfur/carbon composite cathode suffer from sever capacity fade as reported in recent literatures summarized in Table S1, which led to the development of respective complex structures. Therefore, it is worth noting that the performance of LSBs containing such sulfur/carbon composite cathodes could be significantly improved by the addition of a small amount of PEDOT-S@PAN nanofibers as cathode additives. Moreover, this research expresses a new approach to suppress the LiPS shuttle effect through the incorporation of flexible fibrous additives which is different from the previous design strategies of using rigid metal oxide additives and/or complicated host structures containing sulfur.

## 4. Conclusions

In summary, we have developed plant root-like flexible fibrous additives for cathode of LSBs, which not only anchor the LiPS to reduce the shuttling effect, but also restrain the volume variation during cycling. The novel architectures of PEDOT-S@PAN nanofibers are fabricated using a vertical co-axial electrospinning technique followed by post treatment to create the desired morphology. The electrochemical results with the incorporation of PEDOT-S@PAN nanofibers in sulfur cathode of LSB are found to be quite promising in terms of cycle stability and rate capability. Moreover, sulfur lithiation impedance is decreased with the incorporation of a small amount of PEDOT-S@PAN nanofibers. Although we have confirmed the favorable performance of PEDOT-S@PAN nanofiber additives at a minimum content of only 5 wt% as a proof-of-concept in LSB cathode containing 40 wt% active material-sulfur, the performance with varying nanofiber additive content at higher sulfur loadings could also be tested. These results are expected to open doors for innovative design of flexible additives for high energy density LSBs.

## Acknowledgement

This work was supported by the Department of Science and Technology, India (Project No. DST/TMD/MES/2k17/73).

## Appendix A. Supplementary data

SEM image of microtomed longitudinal section of S@PAN nanofiber; TGA data of in-situ synthesized sulfur; FTIR spectra of S@PAN, PEDOT-S@PAN and PEDOT:PSS; SEM image of S/C/PEDOT-S@PAN hybrid cathode; Cycling performance of LSB containing 0, 2.5, 5 and 7.5 wt% S/C/PEDOT-S@PAN hybrid cathode; OCP curve and galvanostatic discharge-charge voltage profile at 0.2 C-rate showing overpotential; FESEM image of S/C/PEDOT-S@PAN hybrid cathode before and after 100 cycles of galvanostatic discharging-charging; EDX elemental mapping of S/C/PEDOT-S@PAN hybrid cathode after 100 cycles of discharging-charging; Digital photograph and UV–vis spectra of cycled separators; EDX spectra of cycled Li anode; Cycling performance of S/C/PEDOT-PAN cathode.

Supplementary data to this article can be found online at https://doi.org/10.1016/j.jpowsour.2019.05.055.

## References

[1] S. Urbonaite, T. Poux, P. Novák, Progress towards commercially viable Li-S battery cells, Advanced Energy Materials 5 (2015) 1500118, https://doi.org/10.1002/aenm.201500118.
[2] A. Rosenman, E. Markevich, G. Salitra, D. Aurbach, A. Garsuch, F.F. Chesneau, Review on Li-sulfur battery systems: an integral perspective, Advanced Energy Materials 5 (2015) 1500212, https://doi.org/10.1002/aenm.201500212.
[3] S. Theivaprakasam, J. Wu, J.C. Pramudita, N. Sharma, D.R. MacFarlane, S. Mitra, Understanding the behavior of $LiCoO_2$ cathodes at extended potentials in ionic liquid–alkyl carbonate hybrid electrolytes, J. Phys. Chem. C 121 (2017) 15630–15638, https://doi.org/10.1021/acs.jpcc.7b05591.
[4] S.-H. Chung, P. Han, A. Manthiram, Quantitative analysis of electrochemical and electrode stability with low self-discharge lithium-sulfur batteries, ACS Appl. Mater. Interfaces 9 (2017) 20318–20323, https://doi.org/10.1021/acsami.7b05602.
[5] Y.-X. Yin, S. Xin, Y.-G. Guo, L.-J. Wan, Lithium-sulfur batteries: electrochemistry, materials, and prospects, Angew. Chem. Int. Ed. 52 (2013) 13186–13200, https://doi.org/10.1002/anie.201304762.
[6] R. Fang, S. Zhao, Z. Sun, D.-W. Wang, H.-M. Cheng, F. Li, More reliable lithium-sulfur batteries: status, solutions and prospects, Adv. Mater. 29 (2017) 1606823, https://doi.org/10.1002/adma.201606823.
[7] S.S. Zhang, Liquid electrolyte lithium/sulfur battery: fundamental chemistry, problems, and solutions, J. Power Sources 231 (2013) 153–162, https://doi.org/10.1016/j.jpowsour.2012.12.102.
[8] J. Zhang, C.-P. Yang, Y.-X. Yin, L.-J. Wan, Y.-G. Guo, Sulfur encapsulated in graphitic carbon nanocages for high-rate and long-cycle lithium-sulfur batteries, Adv. Mater. 28 (2016) 9539–9544, https://doi.org/10.1002/adma.201602913.
[9] Y.V. Mikhaylik, J.R. Akridge, Polysulfide shuttle study in the Li/S battery system, J. Electrochem. Soc. 151 (2004) A1969, https://doi.org/10.1149/1.1806394.
[10] W. Kang, N. Deng, J. Ju, Q. Li, D. Wu, X. Ma, L. Li, M. Naebe, B. Cheng, A review of recent developments in rechargeable lithium–sulfur batteries, Nanoscale 8 (2016) 16541–16588, https://doi.org/10.1039/C6NR04923K.
[11] S. Choudhury, D. Fischer, P. Formanek, M. Stamm, L. Ionov, Phase inversion strategy to fabricate porous carbon for Li-S batteries via block copolymer self-assembly, Advanced Materials Interfaces 5 (2018) 1701116, https://doi.org/10.1002/admi.201701116.
[12] Z. Gong, Q. Wu, F. Wang, X. Li, X. Fan, H. Yang, Z. Luo, A hierarchical micro/mesoporous carbon fiber/sulfur composite for high-performance lithium–sulfur batteries, RSC Adv. 6 (2016) 37443–37451, https://doi.org/10.1039/C6RA04146A.
[13] Y. Zhong, D. Chao, S. Deng, J. Zhan, R. Fang, Y. Xia, Y. Wang, X. Wang, X. Xia, J. Tu, Confining sulfur in integrated composite scaffold with highly porous carbon fibers/vanadium nitride arrays for high-performance lithium-sulfur batteries, Adv. Funct. Mater. 28 (2018) 1706391, https://doi.org/10.1002/adfm.201706391.
[14] X. Shang, P. Guo, T. Qin, M. Liu, M. Lv, D. Liu, D. He, Sulfur immobilizer by nanoscale $TiO_2$ trapper deposited on hierarchical porous carbon and graphene for cathodes of lithium-sulfur batteries, Advanced Materials Interfaces 5 (2018) 1701602, https://doi.org/10.1002/admi.201701602.
[15] J.S. Lee, W. Kim, J. Jang, A. Manthiram, Sulfur-embedded activated multichannel carbon nanofiber composites for long-life, high-rate lithium-sulfur batteries, Advanced Energy Materials 7 (2017) 1601943, https://doi.org/10.1002/aenm.201601943.
[16] Q. Zhu, H. Deng, Q. Su, G. Du, Y. Yu, S. Ma, B. Xu, A free-standing nitrogen-doped porous carbon foam electrode derived from melaleuca bark for lithium-sulfur batteries, Electrochim. Acta 293 (2019) 19–24, https://doi.org/10.1016/j.electacta.2018.10.017.
[17] L. Huang, J. Cheng, X. Li, D. Yuan, W. Ni, G. Qu, Q. Guan, Y. Zhang, B. Wang, Sulfur quantum dots wrapped by conductive polymer shell with internal void spaces for high-performance lithium–sulfur batteries, J. Mater. Chem. 3 (2015) 4049–4057, https://doi.org/10.1039/C4TA06609J.
[18] J.H. Zeng, Y.F. Wang, S.Q. Gou, L.P. Zhang, Y. Chen, J.X. Jiang, F. Shi, Sulfur in hyper-cross-linked porous polymer as cathode in lithium–sulfur batteries with enhanced electrochemical properties, ACS Appl. Mater. Interfaces 9 (2017) 34783–34792, https://doi.org/10.1021/acsami.7b07982.
[19] Z. Cheng, H. Pan, H. Zhong, Z. Xiao, X. Li, R. Wang, Porous organic polymers for polysulfide trapping in lithium-sulfur batteries, Adv. Funct. Mater. 28 (2018) 1707597, https://doi.org/10.1002/adfm.201707597.
[20] Z. Wei Seh, W. Li, J.J. Cha, G. Zheng, Y. Yang, M.T. McDowell, P.-C. Hsu, Y. Cui, Sulphur–TiO2 yolk–shell nanoarchitecture with internal void space for long-cycle lithium–sulphur batteries, Nat. Commun. 4 (2013), https://doi.org/10.1038/ncomms2327.
[21] Q. Sun, B. Xi, J.-Y. Li, H. Mao, X. Ma, J. Liang, J. Feng, S. Xiong, Nitrogen-Doped graphene-supported mixed transition-metal oxide porous particles to confine polysulfides for lithium-sulfur batteries, Advanced Energy Materials 8 (2018) 1800595, https://doi.org/10.1002/aenm.201800595.
[22] L. Yao, X. Dong, C. Zhang, N. Hu, Y. Zhang, Metal oxide nanoprism-arrays assembled in N-doped carbon foamy nanoplates that have efficient polysulfide-retention for ultralong-cycle-life lithium–sulfur batteries, J. Mater. Chem. 6 (2018) 11260–11269, https://doi.org/10.1039/C8TA03012J.
[23] J. He, L. Luo, Y. Chen, A. Manthiram, Yolk-shelled C@$Fe_3O_4$ nanoboxes as efficient sulfur hosts for high-performance lithium-sulfur batteries, Adv. Mater. 29 (2017) 1702707, https://doi.org/10.1002/adma.201702707.
[24] K. Xie, Y. Han, W. Wei, H. Yu, C. Zhang, J.-G. Wang, W. Lu, B. Wei, Fabrication of a novel $TiO_2$/S composite cathode for high performance lithium–sulfur batteries, RSC Adv. 5 (2015) 77348–77353, https://doi.org/10.1039/C5RA13823J.

[25] G. Liang, J. Wu, X. Qin, M. Liu, Q. Li, Y.-B. He, J.-K. Kim, B. Li, F. Kang, Ultrafine $TiO_2$ decorated carbon nanofibers as multifunctional interlayer for high-performance lithium–sulfur battery, ACS Appl. Mater. Interfaces 8 (2016) 23105–23113, https://doi.org/10.1021/acsami.6b07487.
[26] R. Singhal, S.-H. Chung, A. Manthiram, V. Kalra, A free-standing carbon nanofiber interlayer for high-performance lithium–sulfur batteries, J. Mater. Chem. 3 (2015) 4530–4538, https://doi.org/10.1039/C4TA06511E.
[27] Y.-S. Su, A. Manthiram, Lithium–sulphur batteries with a microporous carbon paper as a bifunctional interlayer, Nat. Commun. 3 (2012) 1166, https://doi.org/10.1038/ncomms2163.
[28] D.K. Lee, C.W. Ahn, H.-J. Jeon, Web-structured graphitic carbon fiber felt as an interlayer for rechargeable lithium-sulfur batteries with highly improved cycling performance, J. Power Sources 360 (2017) 559–568, https://doi.org/10.1016/j.jpowsour.2017.06.048.
[29] S. Tu, X. Chen, X. Zhao, M. Cheng, P. Xiong, Y. He, Q. Zhang, Y. Xu, A polysulfide-immobilizing polymer retards the shuttling of polysulfide intermediates in lithium-sulfur batteries, Adv. Mater. 30 (2018) 1804581, https://doi.org/10.1002/adma.201804581.
[30] Y. Peng, Y. Zhang, Y. Wang, X. Shen, F. Wang, H. Li, B.-J. Hwang, J. Zhao, Directly coating a multifunctional interlayer on the cathode via electrospinning for advanced lithium–sulfur batteries, ACS Appl. Mater. Interfaces 9 (2017) 29804–29811, https://doi.org/10.1021/acsami.7b08804.
[31] M.-S. Song, S.-C. Han, H.-S. Kim, J.-H. Kim, K.-T. Kim, Y.-M. Kang, H.-J. Ahn, S. X. Dou, J.-Y. Lee, Effects of nanosized adsorbing material on electrochemical properties of sulfur cathodes for Li/S secondary batteries, J. Electrochem. Soc. 151 (2004) A791, https://doi.org/10.1149/1.1710895.
[32] Y.J. Choi, B.S. Jung, D.J. Lee, J.H. Jeong, K.W. Kim, H.J. Ahn, K.K. Cho, H.B. Gu, Electrochemical properties of sulfur electrode containing nano $Al_2O_3$ for lithium/sulfur cell, Phys. Scripta T129 (2007) 62–65, https://doi.org/10.1088/0031-8949/2007/T129/014.
[33] Y. Zhang, X. Wu, H. Feng, L. Wang, A. Zhang, T. Xia, H. Dong, Effect of nanosized Mg0.8Cu0.2O on electrochemical properties of Li/S rechargeable batteries, Int. J. Hydrogen Energy 34 (2009) 1556–1559, https://doi.org/10.1016/j.ijhydene.2008.12.006.
[34] X. Ji, S. Evers, R. Black, L.F. Nazar, Stabilizing lithium–sulphur cathodes using polysulphide reservoirs, Nat. Commun. 2 (2011) 325, https://doi.org/10.1038/ncomms1293.
[35] K. Xie, Y. You, K. Yuan, W. Lu, K. Zhang, F. Xu, M. Ye, S. Ke, C. Shen, X. Zeng, X. Fan, B. Wei, Ferroelectric-enhanced polysulfide trapping for lithium-sulfur battery improvement, Adv. Mater. 29 (2017) 1604724, https://doi.org/10.1002/adma.201604724.
[36] K. Zhang, L. Wang, W. Cai, C. Wang, G. Li, Z. Li, W. Mao, Y. Qian, A novel class of functional additives for cyclability enhancement of the sulfur cathode in lithium sulfur batteries, Inorganic Chemistry Frontiers 5 (2018) 2013–2017, https://doi.org/10.1039/C8QI00407B.
[37] W. Vannoppen, S. De Baets, J. Keeble, Y. Dong, J. Poesen, How do root and soil characteristics affect the erosion-reducing potential of plant species? Ecol. Eng. 109 (2017) 186–195, https://doi.org/10.1016/j.ecoleng.2017.08.001.
[38] S. Ramakrishna, K. Fujihara, W.-E. Teo, T. Yong, Z. Ma, R. Ramaseshan, Electrospun nanofibers: solving global issues, Mater. Today 9 (2006) 40–50, https://doi.org/10.1016/S1369-7021(06)71389-X.
[39] S. Chen, Y. Gao, Z. Yu, M.L. Gordin, J. Song, D. Wang, High capacity of lithium-sulfur batteries at low electrolyte/sulfur ratio enabled by an organosulfide containing electrolyte, Nanomater. Energy 31 (2017) 418–423, https://doi.org/10.1016/j.nanoen.2016.11.057.
[40] A. Ghosh, R. Manjunatha, R. Kumar, S. Mitra, A facile bottom-up approach to construct hybrid flexible cathode scaffold for high-performance lithium–sulfur batteries, ACS Appl. Mater. Interfaces 8 (2016) 33775–33785, https://doi.org/10.1021/acsami.6b11180.
[41] S. Ahamad, M. Ahmad, B.R. Mehta, A. Gupta, Effect of nano-fillers on capacity retention and rate capability of mesocarbon microbeads anode, J. Electrochem. Soc. 164 (2017) A2967–A2976, https://doi.org/10.1149/2.0351713jes.
[42] D.-G. Yu, X.-Y. Li, X. Wang, J.-H. Yang, S.W.A. Bligh, G.R. Williams, Nanofibers fabricated using triaxial electrospinning as zero order drug delivery systems, ACS Appl. Mater. Interfaces 7 (2015) 18891–18897, https://doi.org/10.1021/acsami.5b06007.
[43] M. Shamsipur, S.M. Pourmortazavi, M. Roushani, I. Kohsari, S.S. Hajimirsadeghi, Novel approach for electrochemical preparation of sulfur nanoparticles, Microchimica Acta 173 (2011) 445–451, https://doi.org/10.1007/s00604-011-0581-8.
[44] A.M. Awwad, N.M. Salem, A.O. Abdeen, Noval approach for synthesis sulfur (S-NPs) nanoparticles using albizia julibrissin fruits extract, Advanced Materials Letters 6 (2015) 432–435, https://doi.org/10.5185/amlett.2015.5792.
[45] J. Lee, W. Choi, Surface modification of sulfur cathodes with PEDOT:PSS conducting polymer in lithium-sulfur batteries, J. Electrochem. Soc. 162 (2015) A935–A939, https://doi.org/10.1149/2.0651506jes.
[46] Y. Liu, D. Sun, S. Askari, J. Patel, M. Macias-Montero, S. Mitra, R. Zhang, W.-F. Lin, D. Mariotti, P. Maguire, Enhanced dispersion of TiO2 nanoparticles in a TiO2/PEDOT:PSS hybrid nanocomposite via plasma-liquid interactions, Sci. Rep. (2015) 5, https://doi.org/10.1038/srep15765.
[47] C. Dillard, A. Singh, V. Kalra, Polysulfide speciation and electrolyte interactions in lithium–sulfur batteries with *in situ* infrared spectroelectrochemistry, J. Phys. Chem. C 122 (2018) 18195–18203, https://doi.org/10.1021/acs.jpcc.8b02506.
[48] H. Li, L. Sun, G. Wang, Self-assembly of polyethylene glycol-grafted carbon nanotube/sulfur composite with nest-like structure for high-performance lithium–sulfur batteries, ACS Appl. Mater. Interfaces 8 (2016) 6061–6071, https://doi.org/10.1021/acsami.5b12496.
[49] G. Hu, Z. Sun, C. Shi, R. Fang, J. Chen, P. Hou, C. Liu, H.-M. Cheng, F. Li, A sulfur-rich copolymer@CNT hybrid cathode with dual-confinement of polysulfides for high-performance lithium-sulfur batteries, Adv. Mater. 29 (2017) 1603835, https://doi.org/10.1002/adma.201603835.
[50] S. Ahamad, A. Gupta, A systematic study of kinetics in mesocarbon microbeads anodes in presence of nano-conductive additives, Electrochim. Acta 297 (2019) 916–928, https://doi.org/10.1016/j.electacta.2018.12.006.
[51] J. Kasnatscheew, U. Rodehorst, B. Streipert, S. Wiemers-Meyer, R. Jakelski, R. Wagner, I.C. Laskovic, M. Winter, Learning from overpotentials in lithium ion batteries: a case study on the $LiNi_{1/3}Co_{1/3}Mn_{1/3}O_2$ (NCM) cathode, J. Electrochem. Soc. 163 (2016) A2943–A2950, https://doi.org/10.1149/2.0461614jes.
[52] D.-H. Lim, M. Agostini, F. Nitze, J. Manuel, J.-H. Ahn, A. Matic, Route to sustainable lithium-sulfur batteries with high practical capacity through a fluorine free polysulfide catholyte and self-standing Carbon Nanofiber membranes, Sci. Rep. 7 (2017), https://doi.org/10.1038/s41598-017-06593-2.
[53] Q. Pang, X. Liang, C.Y. Kwok, L.F. Nazar, Advances in lithium–sulfur batteries based on multifunctional cathodes and electrolytes, Nature Energy 1 (2016), https://doi.org/10.1038/nenergy.2016.132.
[54] J. Guo, Z. Yang, Y. Yu, H.D. Abruña, L.A. Archer, Lithium–sulfur battery cathode enabled by lithium–nitrile interaction, J. Am. Chem. Soc. 135 (2013) 763–767, https://doi.org/10.1021/ja309435f.
[55] A. Jozwiuk, H. Sommer, J. Janek, T. Brezesinski, Fair performance comparison of different carbon blacks in lithium–sulfur batteries with practical mass loadings – simple design competes with complex cathode architecture, J. Power Sources 296 (2015) 454–461, https://doi.org/10.1016/j.jpowsour.2015.07.070.